Quantifying the degree of locking in weakly forced stochastic systems

Jordi Tiana-Alsina, Carlos Quintero-Quiroz, M. C. Torrent, and Cristina Masoller
Departament de Física, Universitat Politècnica de Catalunya, Rambla St. Nebridi 2, 08222 Terrassa, Barcelona, Spain

(Received 18 June 2018; published 12 February 2019)

Controlling an stochastic nonlinear system with a small amplitude signal is a fundamental problem with many practical applications. Quantifying locking is challenging, and current methods, such as spectral or correlation analysis, do not provide a precise measure of the degree of locking. Here we study locking in an experimental system, consisting of a semiconductor laser with optical feedback operated in the regime where it randomly emits abrupt spikes. To quantify the locking of the optical spikes to small electric perturbations, we use two measures, the success rate (SR) and the false positive rate (FPR). The SR counts the spikes that are emitted shortly after each perturbation, while the FPR counts the additional extra spikes. We show that the receiver operating characteristic (ROC) curve (SR versus FPR plot) uncovers parameter regions where the electric perturbations fully control the laser spikes, such that the laser emits, shortly after each perturbation, one and only one spike. To demonstrate the general applicability of the ROC analysis we also study a stochastic bistable system under square-wave forcing and show that the ROC curve allows identifying the parameters that produce best locking.

DOI: 10.1103/PhysRevE.99.022207

I. INTRODUCTION

The entrainment or locking phenomenon, by which an oscillator adapts its natural rhythm to an external periodic signal, is well known [1]. It has been observed in lasers [2–7], chemical systems [8,9], biological oscillators [10–13], circadian cells [14–17], etc. In many situations it is important to gain full control of the system with a small amplitude signal. Examples include periodic electrical stimulation of cardiac tissue for the control of arrhythmias or electrical stimulation of the brain nervous system for the treatment of disorders such as epilepsy or Parkinson's [18–21].

Various control strategies have been proposed in the literature, and a popular one is based on stabilizing an unstable periodic orbit of the system [22]; however, this technique is successful only if the system has an unstable orbit that can be stabilized.

A technical challenge is to quantify the quality of the locking obtained (in particular, in stochastic systems), and precise measures are lacking. The simplest way to identify locking is to measure the oscillation period (the dominant peak of the Fourier spectrum) in units of the forcing period. In this way, when varying the forcing amplitude and period, a pattern of tongues (known as Arnold tongues) is found. In the different tongues the oscillator synchronizes to the external forcing such that the oscillation frequency and the external frequency are related as $pf_{\rm osc} = qf_{\rm ext}$ with p and q being integer numbers. Between Arnold tongues, the system is unlocked and shows aperiodic oscillations. Another well-known tool is the phase-response or phase-resetting curve (PRC), which describes the effect of a perturbation in the phase of the oscillator [23–25]. The PRC simplifies the description of complex, stochastic dynamics to a one-dimensional phase dynamics, allowing us to determine whether the phase of the oscillator is locked to the external signal, but it has the drawback that one needs to estimate the phase, which can be difficult when the oscillator is inherently noisy and/or when its dynamics involves different timescales.

Here we demonstrate that receiver operating characteristic (ROC) curves allow for a precise quantification of the degree of locking. A ROC curve quantifies the diagnostic ability of a binary classifier as a function of its classification threshold. ROC curves (developed during World World II for detecting enemy objects in battlefields) are nowadays routinely used by machine learning algorithms for classification but have not yet been employed, to the best of our knowledge, to quantify locking.

The experimental system used is a semiconductor laser with optical feedback, which displays a rich variety of nonlinear behaviors [26–28]. Here we focus on the so-called low-frequency fluctuations (LFF) regime, where the laser emits a spiking output: during a spike the intensity drops abruptly and then recovers gradually [see Fig. 1(a)]. In this regime, we control the spikes via periodic, small-amplitude electric perturbations of the laser pump current. Using the ROC analysis we find the operation conditions that produce perfect locking: the laser responds to each electrical perturbation with one optical pulse, with no single extra pulse, and with no single missed pulse [Fig. 1(c)]. While the laser with optical feedback and current modulation has been studied in the literature [2–7,29–35], to the best of our knowledge, no perfect locking has yet been reported.

To demonstrate the general applicability of the ROC approach, we also consider a numerical example: a stochastic bistable system with square-wave forcing. In addition, in the Supplemental Material [36] we show that the quantification of the locking quality obtained from the ROC curve is not obtained with other, more direct means (such as the analysis of the interspike-interval distribution, the Fourier spectrum, the cross-correlation, or the autocorrelation function).

II. EXPERIMENTAL SETUP

The experimental setup [35] uses a 685 nm semiconductor laser (Thorlabs HL6750MG) with solitary threshold

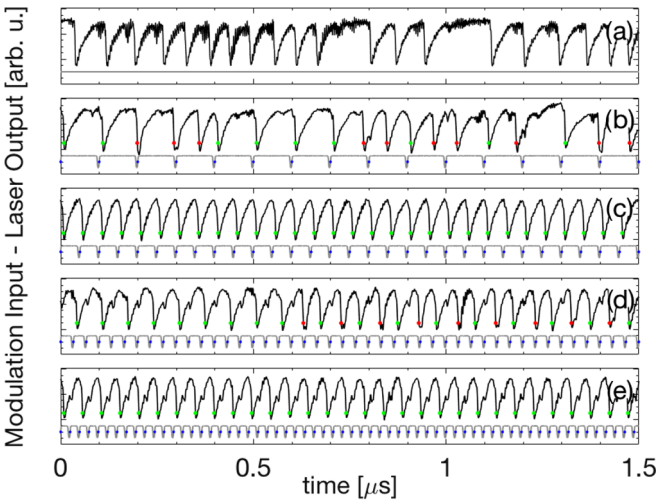

FIG. 1. Time series of the laser intensity (black line, normalized to zero mean and unit variance) and the pulse-down waveform applied to the dc pump current (gray lines, shifted vertically for clarity). Green dots represent the spikes that occur shortly after a perturbation, and red dots mark those spikes that are considered noninduced by a perturbation. The dc pump current is $I_{dc} = 27$ mA, and the modulation amplitude is 2.3% of I_{dc}. (a) The unforced dynamics ($A_{mod} = 0$). For this pump current the natural frequency of the laser spikes is $f_0 = 15$ MHz. (b) The intensity dynamics when $A_{mod} = 2.3\%$ of I_{dc} the perturbation frequency, $f_{mod} = 10$ MHz. (c, e) Locking 1:1 and 2:1 for $f_{mod} = 20$ MHz and 41 MHz, respectively. (d) The transition between locking 1:1 and 2:1 observed at $f_{mod} = 30$ MHz.

$I_{th,sol} = 26.62$ mA, which has part of its output fed back to the laser by a mirror. The feedback produced a 7.2% threshold reduction ($I_{th} = 24.70$ mA). The length of the external cavity is 70 cm, which gives a delay time of 5 ns. The laser temperature and current were stabilized with 0.01 C and 0.01 mA accuracy, respectively. A 90/10 beam-splitter in the external cavity sends light to a photodetector (Det10A/M), an amplifier (Femto HSA-Y-2-40), and a 1 GHz oscilloscope (Agilent DSO9104A). To modulate the laser current we used a 500 MHz Bias-T in the laser mount. The waveform used is a pulse-down periodic signal, as it produces locking for a wide range of parameters [35]. The signal was generated by a function generator (Agilent 81150A), and the duration of the pulse was the shortest available: 5 ns with raising and falling times of 2.5 ns each.

The control parameters are the dc value of the laser current, I_{dc}, which controls the natural frequency of the spikes, f_0, the peak to peak perturbation amplitude, A_{mod}, and frequency, f_{mod}. I_{dc} was varied in the range 25 mA to 28 mA, f_{mod}, in the range 1 MHz to 80 MHz, and A_{mod}, in the range 0.2 mA to 0.62 mA. Therefore, for the lowest I_{dc} value, A_{mod} represents a variation between 0.75% and 2.5% of the dc level, while for the highest dc value, A_{mod} represents a variation between 0.7% and 2.2%. For each set of parameters a time series of the laser intensity with $N = 10^7$ data points was recorded with 2 GS/s sampling rate, which allowed to capture the intensity dynamics during 5 ms.

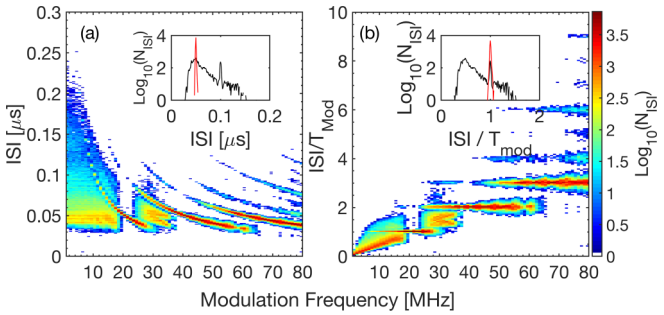

FIG. 2. Interspike interval (ISI) distribution as a function of the perturbation frequency for $I_{dc} = 27$ mA and $A_{mod} = 0.62$ mA (2.3% with respect to I_{dc}). In order to enhance the plot contrast, the color scale indicates the logarithmic of the number of intervals (the white color stands for zero counts). (a) The vertical axis is the ISI (b) it is normalized by the perturbation period. The insets display typical ISI histograms when the laser is mainly driven by its natural dynamics (black line for $f_{mod} = 10$ MHz) and when it is driven by the external perturbations (red line for $f_{mod} = 20$ MHz).

III. EXPERIMENTAL RESULTS

Figure 1 displays typical examples of the intensity dynamics when the laser is not perturbed [Fig. 1(a)] and when it is periodically perturbed [Figs. 1(b) and 1(c)] with $A_{mod} = 2.3\%$ of $I_{dc} = 27$ mA and different frequencies.

The spikes which occur shortly after a current perturbation are considered to be induced by the perturbation and are indicated with green dots (in the following, they will be referred to as *true positives*). The other spikes will be referred to as *false positives* and are indicated with red dots. In Fig. 1(b) the frequency of the perturbations is lower than the natural frequency of the spikes ($f_{mod} = 10$ MHz and $f_0 = 15$ MHz). It is observed that after each perturbation the laser emits a spike, but between perturbations the natural dynamics prevails, and thus, many spikes are spontaneous (false positives). For a higher frequency [Fig. 1(c)] locking 1:1 is observed since every perturbation triggers a spike. For a higher frequency [Fig. 1(d)], there is a transition between locking 1:1 and 2:1. In this region the spikes cannot follow the fast external perturbations, and some spikes are delayed with respect to the perturbations. By further increasing the perturbation frequency, the spike rate adjusts such that there is one spike every two perturbations [Fig. 1(e)].

The variation of the spike rate with the frequency of the external signal is typical of the locking phenomenon. To analyze the locking degree we study the distribution of the time intervals between consecutive spikes [the interspike intervals (ISIs)]. We present in Fig. 2 the ISI distribution (in color code) versus the perturbation frequency, keeping fixed A_{mod} and I_{dc}. The ISI distribution is presented in two ways: in Fig. 2(a) the vertical axis is the time interval between spikes (ISI), while in Fig. 2(b), it is normalized to $T_{mod} = 1/f_{mod}$ (here the histograms are computed with bins centered at nT_{mod}).

In Fig. 2(a), as f_{mod} increases we observe the transition from no locking to 1:1 locking. At low frequencies (from 0 to 15 MHz) the laser behaves as if it is not driven by the external signal and the natural noisy dynamics dominates. This is revealed by a broad ISI distribution, which has only

a small narrow peak at f_{mod} (an example is presented in the inset, black line).

As the frequency increases, the spikes lock to the external signal, and the ISI distribution becomes very narrow, as seen in the insets in Fig. 2 (red lines). In the locking regions the spikes are mainly controlled by the external perturbations, and the ISI distribution peaks at nT_{mod}, where n is an integer number.

A large transition region, characterized by a broad ISI distribution, is observed between locking 1:1 and 2:1. In this region the dynamics is characterized by a reorganization of the spikes, which no longer fit in one period (as in the 1:1 region), but an interval of two periods is too long for a single spike (as in the 2:1 region); see Fig. 1(d). Therefore, after a perturbation, some spikes occur before the next perturbation, while others occur after the next perturbation.

Another feature that can be observed in Fig. 2(a) is that the spike rate cannot be too fast (the smallest ISI is about 0.03 μs). When f_{mod} increases and the most probable ISI reaches this minimum time, the transition to the next locking regime starts. The minimum ISI (referred to as *refractory time*) is due to the fact that after each spike, a steplike recovery occurs, and during the recovery process, another spike is unlikely to be emitted.

In Fig. 2(b) the $nT_{\mathrm{mod}} = \langle \mathrm{ISI} \rangle$ curves are converted into horizontal plateaus due to the normalization by T_{mod}. In this plot it is clearly observed that, as f_{mod} increases, the ISIs become larger multiples of T_{mod} as the laser spikes are spaced by an increasing number of perturbation cycles. At frequencies above 50 MHz the ISI distribution is not unimodal but has several peaks centered at nT_{mod}. This normalized representation of the ISI distribution has the advantage that the locking regions are easy to identify, but the refractory time is not. Due to the normalization, the distribution of the natural spikes (which is independent of f_{mod} in the non-normalized representation of the ISI distribution) is converted in a narrow tilted line, and the broad nature of the ISI distribution at low frequencies is not visible.

In order to quantify the degree of locking we use ROC curves, which are obtained by plotting the true positive rate [TPR, also referred to as success rate (SR)] as a function of the false positive rate (FPR), for different values of the control parameters. The SR measures the response of the laser per perturbation cycle: if the laser emits one spike after each perturbation, SR $= 1$, if it emits one spike every two perturbations, SR $= 1/2$, etc. Only spikes emitted within a detection window of duration τ are considered as spikes induced by the perturbation. The length of the window, $\tau = 15$ ns, is such that only one spike can be emitted within this interval of time [35]. The FPR measures the spikes which are emitted outside this window. FPR $= 0$ indicates that the spikes are always emitted within the interval τ after a perturbation, while FPR $= 1$ indicates that no spike is emitted within this time interval.

The SR versus FPR plots (ROC curves) allow identifying the optimal combination of experimental parameters (A_{mod}, f_{mod}, and I_{dc}) that produce the best locking: if we want to generate an optical spike for each electric perturbation, the optimal parameters are those that give points in the curve that are closest to the top-left corner (i.e., SR $= 1$ and FPR $= 0$).

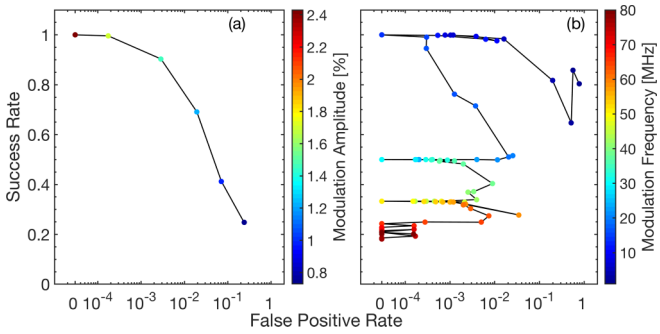

FIG. 3. ROC curve to track transition to locking when (a) the perturbation amplitude increases (in color scale) while keeping constant the frequency ($f_{\mathrm{mod}} = 14$ MHz) and when (b) the perturbation frequency increases (in color scale) while keeping constant the amplitude ($A_{\mathrm{mod}} = 2.4\%$). The dc value of the pump current is $I_{\mathrm{dc}} = 26$ mA. To represent in logarithmic scale the value FPR $= 0$, we have set it to 3×10^{-5} (labeled as 0 in the x axis).

Figure 3(a) displays the transition to locking 1:1 when the perturbation amplitude is increased while the frequency is kept constant (iso-frequency line with $f_{\mathrm{mod}} = 14$ MHz). We note that we reach perfect 1:1 locking (SR $= 1$ and FPR $= 0$) for $A_{\mathrm{mod}} = 2.4\%$. Figure 3(b) displays the transition as f_{mod} increases (iso-amplitude line with $A_{\mathrm{mod}} = 2.4\%$). Here the transitions from SR $= 1$ and FPR $= 0$ to SR $= 1/2$ and FPR $= 0$, and from SR $= 1/2$ and FPR $= 0$ to SR $= 1/3$ and FPR $= 0$, are observed. During these transitions there is an increase of the number of false positives, followed by a decrease, which are due, as discussed before, to the reorganization of the spikes: the spikes cannot follow the external signal as it becomes faster.

Figure 4 displays the ROC curves for four dc values of the pump current. In each panel we plot the SR and FPR values obtained for all the amplitudes and frequencies studied. For easy visualization we join the points with iso-frequency

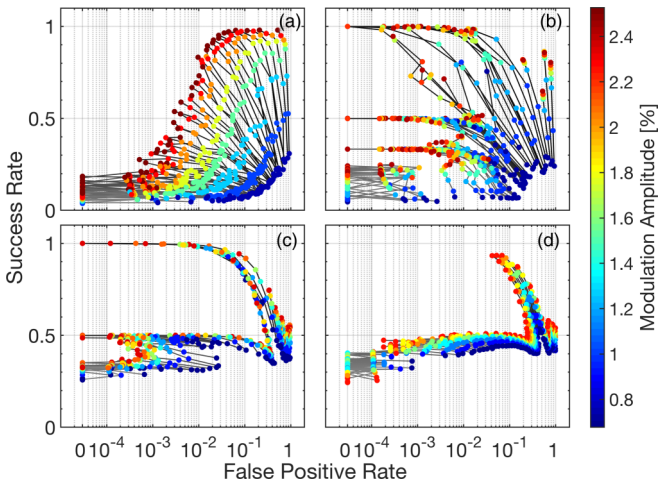

FIG. 4. ROC curves for (a) $I_{\mathrm{dc}} = 25$ mA, (b) 26 mA, (c) 27 mA, and (d) 28 mA. The lines join points with the same perturbation frequency, while the color scale represents the amplitude in percent of I_{dc}. To represent in the logarithmic scale the value FPR $= 0$, we have set it to 3×10^{-5} (labeled as 0 in the x axis).

lines [as in Fig. 3(a)] while the color indicates the amplitude of the perturbation. In Fig. 4(a) we see that for low I_{dc} it is not possible to perfectly entrain the spikes: while the success rate can approach to 1 (at low f_{mod}), the number of false positives is always large (revealing many "natural," uncontrolled spikes). At intermediate I_{dc} values [Figs. 4(b) and 4(c)] there is perfect locking, as indicated by points at SR $= 1, 1/2$ and $1/3$ and FPR $= 0$. For higher I_{dc} [Fig. 4(d)] high-quality locking is not obtained.

IV. NUMERICAL RESULTS

To demonstrate the general applicabilty of ROC analysis, we study numerically a stochastic bistable system [37], $dx/dt = x - x^3 + \sqrt{2D}\xi(t) + F(t)$, where $F(t)$ represents a square-wave periodic signal of amplitude A_{mod} and frequency f_{mod}, and $\xi(t)$ represents white Gaussian noise of strength D. We keep A_{mod} small enough such that, without noise, the square-wave signal does not induce switchings.

With noise, in response to the combined effect of the square-wave signal and the noise, the system switches between two states $(+1, -1)$ and displays optimal switching regularity for particular parameter values (the well-known phenomenon of stochastic resonance [38–40]). Let us next analyze the dynamics using the ROC approach, which allows us to identify the parameters that produce optimal locking, such that the system switches between the two states following the changes of the external signal. To this end, the switchings that follow the changes of the square-wave signal are considered true positives, and the others, false positives.

Figure 5(a) displays the ROC curve obtained when varying the noise strength D, while keeping constant A_{mod} and f_{mod}. At low noise intensities the system rarely switches, and therefore, both SR and FPR are close to 0. As D increases, SR increases while FPR remains low. As D is increased further, SR remains nearly constant while FPR increases due to extra switchings. Remarkably, the noise strength for which the ROC curve is closest to the [0,1] corner coincides with the minimum of the coefficient of variation, C_v, shown in the inset of Fig. 5(a). Thus, ROC analysis identifies optimal switching regularity (i.e., stochastic resonance). This is not the case in Fig. 5(b), where we vary the modulation frequency while keeping constant D and A_{mod}. At f_{mod} there is a high success rate, but also a large number of false positives (extra switchings). As f_{mod} increases, FPR decreases but SR also decreases due to the fact that the system does not always follow the modulation. In contrast to the experimental laser system, in the bistable system we have not found parameters that produce perfect locking. The inset in Fig. 5(b) displays C_v as a function of f_{mod}, and we note it is minimum for $f_{mod} = 0.007$. On the other hand, the frequency for which the ROC curve is closest to the [1,0] corner is $f_{mod} = 0.012$. The system evolution for these frequencies is shown in Figs. 5(c) and 5(d), where we note that, for f_{mod} that minimizes C_v, there are several very short

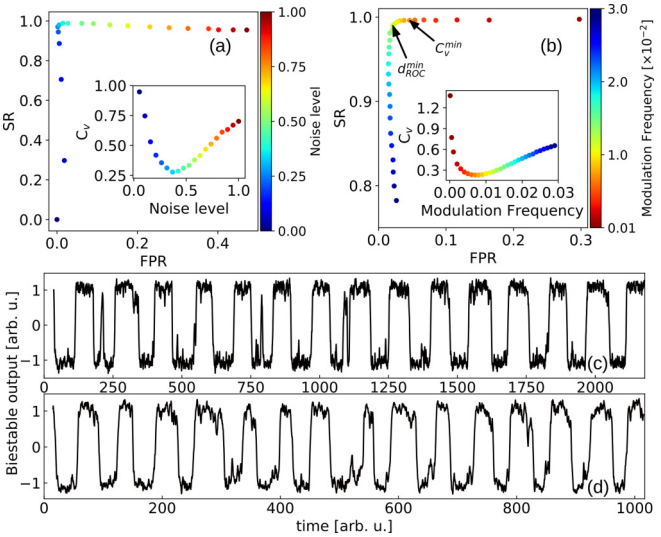

FIG. 5. ROC analysis of a stochastic bistable system with square-wave forcing when the noise strength is varied (a), while keeping constant $A_{mod} = 0.3$ and $f_{mod} = 0.012$, and when the modulation frequency is varied (b), while keeping constant $D = 0.3$ and $A_{mod} = 0.3$. The insets show the coefficient of variation. (c, d) The evolution of the system for the frequency that minimizes C_v, and for the frequency that gives (SR, FPR) closest to the (1, 0) corner.

switchings (e.g., just before 250, shortly after 750 and 1000), which are false positives that do not occur when the system is modulated at the frequency identified by ROC analysis.

V. CONCLUSIONS

To summarize, we have shown that ROC curve analysis provides a precise quantification of the degree of locking of noisy oscillators. In the case of the laser with optical feedback, we have found the experimental parameters that allow full control of the laser output, entraining the emitted spikes to the electric perturbations such that the success rate is equal to 1, while the false positive rate is equal to zero. Considering, as a numerical example, a stochastic bistable system driven by a square-wave periodic force, we have shown that ROC curve analysis allows to identify the parameter for which the system optimally follows the switchings of the forcing signal. We anticipate that ROC curve analysis will lead to higher locking quality in a wide variety of practical applications where irregular oscillations need to be controlled by small amplitude signals.

ACKNOWLEDGMENTS

This work was supported in part by the Spanish MINECO/FEDER (FIS2015-66503-C3-2-P). C.M. also acknowledges partial support from ICREA ACADEMIA, Generalitat de Catalunya.

[1] A. Pikovsky, M. Rosenblum, J. Kurths, and J. Kurths, *Synchronization: A Universal Concept in Nonlinear Sciences*, Vol. 12 (Cambridge University Press, Cambridge, 2003).

[2] D. Baums, W. Elsässer, and E. O. Göbel, Phys. Rev. Lett. **63**, 155 (1989).

[3] J. Sacher, D. Baums, P. Panknin, W. Elsässer, and E. O. Göbel, Phys. Rev. A **45**, 1893 (1992).

[4] P. M. Varangis, A. Gavrielides, T. Erneux, V. Kovanis, and L. F. Lester, Phys. Rev. Lett. **78**, 2353 (1997).
[5] Y. Takiguchi, Y. Liu, and J. Ohtsubo, Opt. Lett. **23**, 1369 (1998).
[6] D. W. Sukow and D. J. Gauthier, IEEE J Quantum Electron. **36**, 175 (2000).
[7] M. Turconi, B. Garbin, M. Feyereisen, M. Giudici, and S. Barland, Phys. Rev. E **88**, 022923 (2013).
[8] A. Zlotnik, Y. Chen, I. Z. Kiss, H.-A. Tanaka, and J.-S. Li, Phys. Rev. Lett. **111**, 024102 (2013).
[9] A. Zlotnik, R. Nagao, I. Z. Kiss, and J.-S. Li, Nat. Commun. **7**, 10788 (2016).
[10] M. Feingold, D. L. Gonzalez, O. Piro, and H. Viturro, Phys. Rev. A **37**, 4060 (1988).
[11] A. T. Winfree, *The Geometry of Biological Time* (Springer, New York, 2001).
[12] P. Lakatos, G. Karmos, A. D. Mehta, I. Ulbert, and C. E. Schroeder, Science **320**, 110 (2008).
[13] K. Pyragas, A. P. Fedaravičius, T. Pyragienė, and P. A. Tass, Phys. Rev. E **98**, 042216 (2018).
[14] M. R. Guevara and L. Glass, J. Math. Biol. **14**, 1 (1982).
[15] H. Zeng, Z. Qian, M. P. Myers, and M. Rosbash, Nature (London) **380**, 129 (1996).
[16] K.-A. Stokkan, S. Yamazaki, H. Tei, Y. Sakaki, and M. Menaker, Science **291**, 490 (2001).
[17] M. Monti, D. K. Lubensky, and P. R. ten Wolde, Phys. Rev. E **97**, 032405 (2018).
[18] P. Tass, M. G. Rosenblum, J. Weule, J. Kurths, A. Pikovsky, J. Volkmann, A. Schnitzler, and H.-J. Freund, Phys. Rev. Lett. **81**, 3291 (1998).
[19] C. Hammond, H. Bergman, and P. Brown, Trends Neurosci. **30**, 357 (2007).
[20] R. Fisher, V. Salanova, T. Witt, R. Worth, T. Henry, R. Gross, K. Oommen, I. Osorio, J. Nazzaro, D. Labar *et al.*, Epilepsia **51**, 899 (2010).
[21] H. Cagnan, D. Pedrosa, S. Little, A. Pogosyan, B. Cheeran, T. Aziz, A. Green, J. Fitzgerald, T. Foltynie, P. Limousin, L. Zrinzo, M. Hariz, K. J. Friston, T. Denison, and P. Brown, Brain **140**, 132 (2017).
[22] E. Ott, C. Grebogi, and J. A. Yorke, Phys. Rev. Lett. **64**, 1196 (1990).
[23] R. F. Galán, G. B. Ermentrout, and N. N. Urban, Phys. Rev. Lett. **94**, 158101 (2005).
[24] T. Netoff, M. A. Schwemmer, and T. J. Lewis, *Phase Response Curves in Neuroscience* (Springer, New York, 2012), p. 95.
[25] F. S. Matias, P. V. Carelli, C. R. Mirasso, and M. Copelli, Phys. Rev. E **95**, 052410 (2017).
[26] J. Mork, B. Tromborg, and J. Mark, IEEE J. Quantum Electron. **28**, 93 (1992).
[27] J. Ohtsubo, *Semiconductor Lasers: Stability, Instability and Chaos* (Springer, New York, 2012).
[28] M. Sciamanna and K. A. Shore, Nat. Phot. **9**, 151 (2015).
[29] M. Giudici, C. Green, G. Giacomelli, U. Nespolo, and J. R. Tredicce, Phys. Rev. E **55**, 6414 (1997).
[30] J. M. Mendez, R. Laje, M. Giudici, J. Aliaga, and G. B. Mindlin, Phys. Rev. E **63**, 066218 (2001).
[31] Y. Hong and K. A. Shore, Opt. Lett. **30**, 3332 (2005).
[32] J. P. Toomey, D. M. Kane, M. W. Lee, and K. A. Shore, Opt. Exp. **18**, 16955 (2010).
[33] T. Sorrentino, C. Quintero-Quiroz, A. Aragoneses, M. C. Torrent, and C. Masoller, Opt. Exp. **23**, 5571 (2015).
[34] K. Hicke, D. Brunner, M. C. Soriano and I. Fischer, Chaos **27**, 114307 (2017).
[35] J. Tiana-Alsina, C. Quintero-Quiroz, M. Panozzo, M. Torrent, and C. Masoller, Opt. Exp. **26**, 9298 (2018).
[36] See Supplemental Material at http://link.aps.org/supplemental/10.1103/PhysRevE.99.022207 for a discussion of other approaches for the quantification of the degree of locking.
[37] B. Shulgin, A. Neiman, and V. Anishchenko, Phys. Rev. Lett. **75**, 4157 (1995).
[38] S. Fauve and F. Heslot, Phys. Lett. A **97**, 5 (1983).
[39] L. Gammaitoni, P. Hänggi, P. Jung, and F. Marchesoni, Rev. Mod. Phys. **70**, 223 (1998).
[40] R. Benzi, A. Sutera, and A. Vulpiani, J. Phys. A **14**, L453 (1981).